

ASSESSING THE SONIC BOOM OF A FULL-SIZE AIRCRAFT FROM FREE FLIGHT TESTS ON A SUB-SCALE MODEL

Giovanni Fasulo¹, Luigi Federico¹

¹Italian Aerospace Research Centre (CIRA), 81043, Capua, Italy

Abstract

In spite of the limited success of the Concorde, the last two decades have seen a resurgence of interest in commercial supersonic flight. In this context, the European Commission has funded the MORE&LESS project, under the Horizon 2020 plan, to assess the potential of some innovative high-speed aircraft configurations and to identify and mature the technologies needed to overcome the main obstacles to their deployment. Since the cost of conducting flight tests is proportional to the size and weight of the aircraft, the use of small unmanned sub-scale models to characterize the sonic boom of the full-scale aircraft is a more desirable option. For this purpose, considerable effort has been devoted to defining a hybrid scaling concept for the sonic boom, combining Whitham's modified linear theory, free flight tests on sub-scale models, and a simplified propagation model. As a result, a cost-effective, simplified, and rapid procedure for the estimation of ground N-waves generated by full-size aircraft has been established.

Keywords: Sonic boom; Ballistic range; Scale model; N-wave.

1. Introduction

Although there are currently no supersonic civil aircraft in operation, significant research efforts are underway to develop new vehicles capable of revolutionizing the current concept of business and tourist air travel, especially in terms of reducing flight times and increasing the number of long-haul routes. However, unlike Concorde, the design phase of new aircraft brings with it new challenges that were not as important at the time. These include ensuring economic viability, environmental sustainability and human acceptance. In this context, the European Commission, under the Horizon 2020 Program and the natural follow-up to a series of European projects (ATLLAS I/II [1], LAPCAT I/II [2], HIKARI [3], HEXAFLY [4], HEXAFLY Int. [5], STRATOFLY [6]), has funded the MOREandLESS project [7] to assess the potential of some innovative high-speed aircraft configurations and to identify and mature the technologies needed to overcome the main obstacles to their deployment. The STRATOFLY MR3 represents the main concept of this framework, namely a highly integrated system capable of flying long-distance routes, reaching Mach 5 in the cruise phase at an altitude of 30-35 km, and carrying many more passengers than the historic Concorde.

In particular, an important driver for the resurgence of civil supersonic aircraft lies in the development of a new low-boom generation aircraft [8, 9] and the establishment of supersonic overflight noise certification standards [10]. In both cases, accurate testing will be very valuable and experimental measurements of sonic boom signatures to representative flight conditions using a full-scale aircraft would be the ideal test procedure. Unfortunately, the costs of developing flight test vehicles are proportional to their size and weight, making a full-scale demonstrator very expensive [11]. Furthermore, practical considerations may prevent the use of this approach for many configurations in any case, necessitating laboratory tests on small subscale models. However, conventional procedures for experimentally measuring the overpressure signature, such as using a wind tunnel, present various limitations. For instance, to characterize the far-field sonic boom, a very small model is required and to fabricate such model, with the necessary geometric fidelity to represent a real aircraft, is extremely challenging, especially considering the boundary layer effect and model vibrations [12]. In addition, as wind tunnel testing techniques could introduce distortion, certain

procedures are required to adjust the measured pressure signature [13]. Therefore, conducting experimental sonic boom tests using small-scale models launched in a ballistic range may be more appropriate. It should be noted that launching a perfectly scaled aircraft model in any ballistic facility poses real difficulties, especially in acquiring steady-level flight conditions. Indeed, minor modifications are usually required to make them into targets. In these cases, it is crucial to carefully consider the influence of geometric adjustment on acoustic properties. Moreover, the utilization of commercial transducers typically yields high-quality pressure signatures, however, there are some limitations, such as nonlinearity in sensitivity and ringing due to the mechanical resonance associated with the diaphragm, which can slightly affect acoustic measurements [14]. Thus, due to the potential of the ballistic range technique, a significant amount of effort was dedicated to establish a scaling concept for the sonic boom, combining Whitham's modified linear theory [15-18], free flight tests on sub-scale models at ground, and a simplified propagation model [19].

Concerning the possibility to replicate the sonic boom from a full-scale aircraft by means of measurements carried out on subscale aircraft, some procedures have already been explored and make available in the literature [11,12,20]. In briefly, they expect to use a subscale model to produce a sonic boom with the same duration and overpressure as a full-scale aircraft, or to produce a scaled sonic boom to then predict the full-scale sonic boom. However, both require flying at relatively high altitudes, i.e., a catapults or launcher systems are needed. Moreover, in other cases, a probing aircraft is required, which introduce another cost. Therefore, the possibility to estimate the ground signature of full-size aircraft from the combination of experimental results on sub-scale model from free-flight tests at ground, theoretical estimation on full-size aircraft and a simple propagation model, made it possible to establish a cost-effective, simplified and rapid procedure for estimating the ground N-waves of full-scale aircraft.

2. Sonic Boom Scaling

2.1 Whitham's Modified Linear Theory

Generally, any object that moves through the air, at speeds exceeding the local speed of sound, produces a system of shock waves attached to its body [21]. Specifically, a body with simple geometry (such as axisymmetric projectiles) typically produces two shock waves: a bow shock wave, attached to the front of the body and a tail shock wave, attached to the rear part of the body. Instead, a body characterized by complicated geometry, such as an aircraft, generally generates a larger number of shock waves. At very large distances, these shock waves tend to coalesce into two shock waves, creating an N-wave signature, as in the case of simpler geometries. In the far field, the bow shock of the N-wave signature corresponds to a rapid local air compression, followed by an expansion until a value below the atmospheric pressure, and then sudden recompression at the tail shock (Figure 1). The sound associated with such a pressure change is called a sonic boom. It is important to note that the pressure signature and so also the sonic boom move with the aircraft and are associated with continuous supersonic flight, not just with "breaking" the sound barrier.

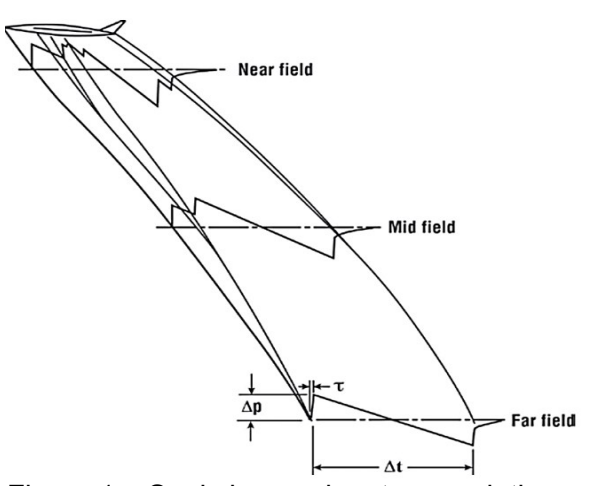


Figure 1 – Sonic boom signature evolution.

According to Whitham's linear theory, if the flow is homogeneous, inviscid, and supersonic, and the body is slender, sufficiently smooth, and the distance from the body is sufficiently large, the flow perturbations can be expressed as integrals of the source distribution and related to a body area distribution [15]:

$$F_W(y) = \frac{1}{2\pi} \int_0^y \frac{A''(\xi)}{\sqrt{y - \xi}} d\xi \tag{1}$$

However, for bodies characterized by discontinuities in the surface slope, Lighthill's more general solution [18] must be used:

$$F_L(y) = \frac{1}{2\pi} \int_0^\infty \sqrt{\frac{2}{\beta R(\xi)}} h\left(\frac{y-\xi}{\beta R(\xi)}\right) dA'(\xi)$$
 (2)

where β is the Prandtl-Glauert coefficient of compressibility and $R(\xi)$ is approximated to $\sqrt{A(\xi)} \setminus \pi$. While the h(z) function has a value of:

$$h(z) = \sqrt{\frac{\pi}{2p}} \frac{1}{K_1(p)} H(z)$$
 (3)

 K_1 is the modified Bessel function of the second kind, p is the Heaviside's operator of differentiation and H(z) is the Heaviside unit step function. Specifically, the function h(z) is plotted in Figure 2:

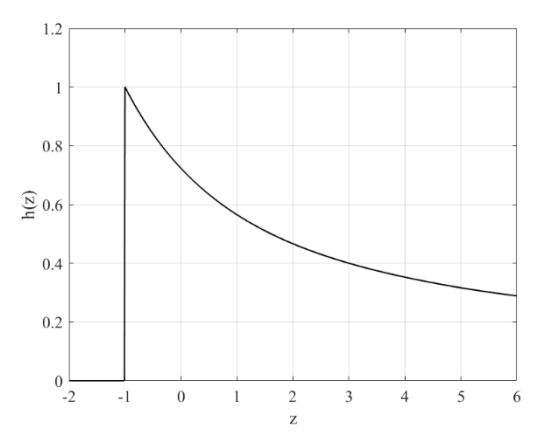


Figure 2 – Function h(z).

The first order solution for the pressure field is expressed as follows in both cases:

$$\Delta p = \frac{p_{\infty} \gamma M_{\infty}^2}{\sqrt{2\beta r}} F(y) \tag{4}$$

where:

- γ is the ratio of specific heats (1.4 for air);
- p_{∞} is the reference pressure for a uniform atmosphere;
- M_{∞} is the flow Mach number;
- r is the minimum distance from model to probe;

It should be noted that these equations are written for axisymmetric and non-lifting bodies. However, Hayes [16] suggests that to represent the complex geometry of an aircraft, the area distribution can be seen as an equivalent area distribution of a revolution slender body based on the longitudinal development of the aircraft's volume and lift.

$$A(y,\phi) = A_y(y,\phi) + A_l(y,\phi) \tag{5}$$

In particular, to account for locally axisymmetric flow, the equivalent area is evaluated using the supersonic area rule concept (Figure 3). According to this rule, the cross-sectional area due to volume, at any station, is determined by the frontal projection of the area intercepted by a cutting plane inclined

at the Mach angle, aligned with ϕ (the azimuth path angle, i.e., the angle in the roll direction) and passing through the longitudinal axis at the airplane station [22]. Instead, according to Walkden [17], the pressure perturbations caused by lift can be estimated solving for the intercept of the Mach cutting planes and the wing camber surface (Figure 3) and integrates the lifting pressures $l(x, \xi, \phi)$ along such line to determine the lift projection component normal to the free stream, in the ξ position and in the ϕ direction. A subsequent longitudinal integration is required to determine the accumulated lifting force at the desired point on the equivalent body axis:

$$A_{l}(y,\phi) = \frac{\beta}{2q} \int_{0}^{y} \int_{x_{1}}^{x_{2}} l(x,\xi,\phi) \, dx d\xi \tag{6}$$

q indicates the dynamic pressure.

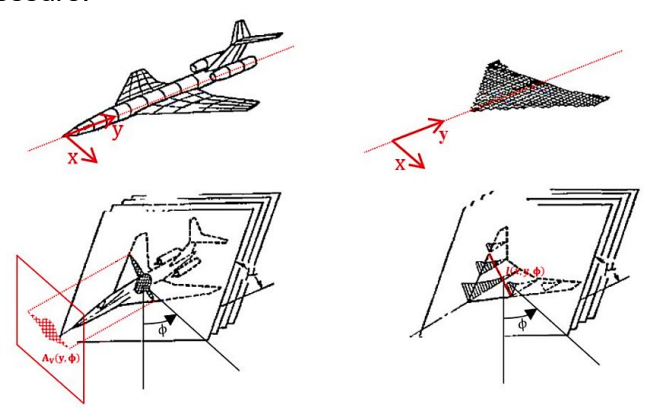


Figure 3 – Supersonic area-rule concept.

The linearized theory above explained provides a correct first approximation of pressure perturbations. However, it cannot predict the location of shocks due to the linearity of the characteristic curve (consequence of the small perturbation assumption, which ensures that the curvature is of small order). Real flow characteristics are instead represented by curves. Indeed, the signature regions of high pressure present a relatively higher speed of sound, which causes them to advance faster than other signal segments and thus leads to an overlap of some parts of the pressure signal. When several characteristics merge, a shock must necessarily be formed since it is physically impossible to associate more than one pressure value at a certain point of space.

Therefore, to address local flow variations, Whitham proposed a correction to the linear characteristic curve by introducing the following non-linear term:

$$y = x - \beta r + \frac{(\gamma + 1)M^4}{\sqrt{2\beta^3}} F(y) \sqrt{r}$$
(7)

Unlike the evolution of straight lines characteristics, the curves characteristics evolution explains the shocks formation, predicts which ones will overtake others with distance, and demonstrates that at very large distances only two shocks will remain with a linear variation of pressure between them (known as an N-wave) [23]. In particular, when considering a flow far enough away from the body, typically beyond several hundred body diameters, such that the signature has evolved into the N-wave, it is possible to obtain simplified analytical solutions for the shock strength and duration [17]:

$$\Delta P = \frac{2^{1/4} \gamma p_{\infty} (M_{\infty}^2 - 1)^{1/8}}{(\gamma + 1)^{1/2}} \sqrt{\int_{0}^{y_{0}} F(y) dy} r^{-3/4}$$
 (8)

$$\Delta t = 2 \frac{2^{1/4} (\gamma + 1)^{1/2} M_{\infty}}{a (M_{\infty}^2 - 1)^{3/8}} \sqrt{\int_0^{y_0} F(y) dy} r^{1/4}$$
(9)

Note that the far field assumption results in a change of the decay law from $r^{-1 \setminus 2}$ to $r^{-1 \setminus 4}$ and the F-function appears only as an integral. In these equations, y_0 represents the y value for which the

integral of F(y) is maximum and a represents the speed of sound.

2.2 Aircraft Shape Factors

Considering the far-field N-wave signatures, which are common to most supersonic aircraft, simplifies theoretical calculations by condensing sonic boom characteristics into a single line on a parametric chart. Specifically, the factor governing the generation of the sonic boom depends mainly on the configuration shape and the aircraft lift, and can be defined as follows:

$$K_S = \frac{2^{1/4} \gamma}{(\gamma + 1)^{1/2}} \frac{\sqrt{\int_0^{y_0} F(y) \, dy}}{l^{3/4}} \tag{10}$$

By substituting the relationship for the aircraft shape factor in Equations (8,9), an estimate of the N-wave can be obtained:

$$\Delta P = K_{\rm S} \, p_{\infty} (M_{\infty}^2 - 1)^{1/8} \, l^{3/4} \, r^{-3/4} \tag{11}$$

$$\Delta t = K_S \frac{2(\gamma + 1)}{\gamma} \frac{M_{\infty}}{a(M_{\infty}^2 - 1)^{1/8}} l^{3/4} r^{-1/4}$$
(12)

The aircraft shape factor can be determined by first evaluating the area distribution and then using Equations (1) or (2) to compute the F-function. Specifically, to accommodate the possibility of non-axisymmetric body studies, F(y) can be generalized to $F(y,\phi)$.

Since the second derivative and the integral are linear mathematical operations, the Whitham F-function can be split into two sub-F-functions: one related to the volume contribute and one associated to the lift contribute.

$$F_{W}(y,\phi) = \frac{1}{2\pi} \int_{0}^{y} \frac{A''(\xi,\phi)}{\sqrt{y-\xi}} d\xi = \frac{1}{2\pi} \int_{0}^{y} \frac{A''_{v}(\xi,\phi) + A''_{l}(\xi,\phi)}{\sqrt{y-\xi}} d\xi = F_{W,v}(y,\phi) + F_{W,l}(y,\phi)$$
(13)

Similarly, the "global" aircraft shape factor can be divided into two components according to the following definitions:

$$K_{S_v}(\phi) = \frac{2^{1/4} \gamma}{(\gamma + 1)^{1/2}} \frac{\sqrt{\int_0^{y_0} F_{W,v}(y,\phi) \, dy}}{l^{3/4}}$$
(14)

$$K_{S_l}(\phi) = \frac{2^{1/4} \gamma}{(\gamma + 1)^{1/2}} \frac{\sqrt{\int_0^{y_0} F_{W,l}(y, \phi) \, dy}}{l^{3/4}}$$
 (15)

Considering y_0 as the y value for which the integral of the sum of the two F-functions is maximum, a relationship can be introduced between the "global" aircraft shape factor and the aircraft shape factors resulting from volume and lift:

$$K_{S} = \sqrt{K S_{\nu}^{2} + K S_{l}^{2}} \tag{16}$$

2.3 Scaling Concept

For a slender, right-cylinder cone which extends to infinity with an apex half-angle of ϵ , the area distribution due to volume can be approximated by the cross-sectional area [21]:

$$A_{\nu}(y) = \pi \epsilon^2 y^2 \tag{17}$$

Since the slender cone is obviously smooth, it is possible to compute the analytical Whitham's F-function using the Equation (1):

$$F_W(y) = 2\epsilon^2 \sqrt{y} \tag{18}$$

When the cone exhibits a finite length, joined for example to another body of cylindrical shape, a flow expansion occurs at the junction. This results in a discontinuous drop at a certain value of y in the F-function defined in Equation (18), followed by a successively smooth recovery to zero. As demonstrated by Ritzel [18], it is possible to obtain an analytical measure of the length of the N-wave positive phase for this simple case:

$$y_0 - y_s^t = \sqrt{\frac{8}{3}k \,\epsilon^2 y_0^{3/2} \,r^{1/4}} \tag{19}$$

The variable y_s^t represents the location of the shock, while the k factor has a value of:

$$k = \frac{(\gamma + 1)M_{\infty}^4}{\sqrt{2}\,\beta^{3/2}}\tag{20}$$

The hybrid scaling concept for the sonic boom assumes that experimental measurements are gathered in a ballistic range, with acoustic transducers positioned far enough from the fire line in order to fall in the far-field region and measure N-wave signatures. In addition, a relatively lightweight scale model needs to be launched at high speed in order to confidently neglect the area contribution due to lift. In these cases, the N-wave time duration measurements can be used to identify an equivalent slender, right-cylinder cone of finite length that accounts for the scaled model volume contribution:

$$y_0 - y_s^t = \frac{\Delta t_{Exp}}{2} M_\infty a \tag{21}$$

According to Equation (18), the Whitham F-function for a slender cone is always monotonically increasing. Moreover, due to the sudden drop in flow expansion at the junction between the cone and the cylinder, y_0 can be set equal to the cone length, which equals the scale model length. Thus, Equation (21) can be substituted into Equation (19) and inverted to obtain a tuned apex half-angle:

$$\epsilon = \frac{\Delta t_{Exp} M_{\infty} a}{2\sqrt{\frac{8}{3}} k \ l^{3/2}} r^{-1/4} \tag{22}$$

In the equation, r is defined as the minimum distance between the fire line and the location of the acoustic transducer.

This model will serve as the baseline for defining a hybrid F-function ("hybrid" adjective indicates that the shape of the F-function is based on theory, while the amplitude is governed by experimental results) and then for estimating an aircraft shape factor from Equation (14). Note that the calculated factor does not depend on the dimensions of the model, but rather on its shape. Therefore, if the model is obtained purely from a scaling procedure applied to the real aircraft, such a value represents a very good estimate of the volume contribution due to the full-size vehicle's volume. Regarding the lift development of the full-size aircraft, it is not feasible to extract valuable information on the area contribution from experimental data, as it is assumed to be negligible. Thus, to assess the global aircraft shape factor, Equation (6) must be used to estimate the aircraft shape factor due to lift. To simplify this procedure and reduce the need for a computer program, a reasonably accurate approximation of the lift distribution can be defined by the planform area distribution, assuming a normal cut and a uniform lift distribution [19]:

$$A_l(y,\phi) = \frac{\beta W \cos(\phi) \cos(\gamma_p)}{2qS} \int_0^y b(\xi) d\xi = \frac{\beta W \cos(\phi) \cos(\gamma_p)}{1.4 p_v M_{co}^2 S} \int_0^y b(\xi) d\xi$$
 (23)

where, $b(\xi)$ is the local span of aircraft wings planform at a given value of ξ -coordinate (along y-axis), W is the aircraft weight, γ_p is the flight-path angle, p_v is the atmospheric pressure at aircraft altitude and S is the total wings aircraft planform area. In addition, defining the lift parameter k_l as:

$$k_l = \frac{\beta W \cos(\phi) \cos(\gamma_p)}{1.4 \ p_v M_{\odot}^2 l^2} \tag{24}$$

the area distribution due to lift can be rewritten as follows:

$$A_{l}(y,\phi) = k_{l} \frac{l^{2}}{S} \int_{0}^{y} b(\xi) d\xi$$
 (25)

However, even if normal cutting could be an acceptable approximation due to the slenderness of the body, the assumption of a uniform lift distribution strongly depends on the type of aircraft (see Figure 4). Therefore, in order to maintain the simplicity of the Carlson equation while ensuring accuracy of results, a modification is proposed. Specifically, it is suggested to calculate the area distribution due to lift using Equation (25) separately for each lifting surface that presents roughly the same lift coefficient (Figure 4).

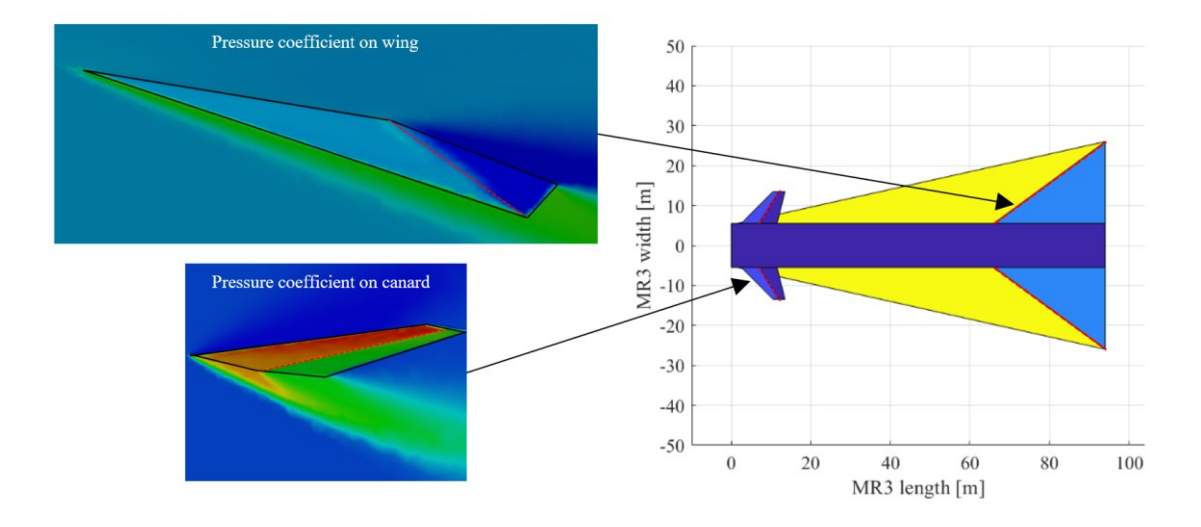


Figure 4 – Pressure coefficient for some lifting surfaces of MR3 [24] and relationship with the proposed approach in computing area due to lift.

Assuming that each surface characterized by a homogeneous lift distribution accounts for a portion of the total weight, it is easy to demonstrate that the corresponding lift development for each surface needs to be modulated by a factor of $W_i \setminus W_{tot}$. Here, i indicates the i-th surface, W_i represents the portion of the total weight accounted for by the i-th surface (or, equally, the lift generated by the i-th surface), and W_{tot} represents the aircraft weight. The sum of all W_i must be equal to W_{tot} . Therefore, maintaining the same formalism, the area distribution due to lift from Equation (25) becomes:

$$A_{l}(y,\phi) = \sum_{i} A_{l_{i}}(y,\phi) = k_{l} \sum_{i} \frac{W_{i}}{W_{tot}} \frac{l^{2}}{S_{i}} \int_{0}^{y} b_{i}(\xi) d\xi = k_{l} \sum_{i} \frac{C_{L_{i}}}{C_{L}} \frac{l^{2}}{S} \int_{0}^{y} b_{i}(\xi) d\xi$$
(26)

where C_L is the lift coefficient. Then Equations (1) or (2) can be used to calculate the F-function, and Equation (15) can be applied to estimate the shape factor of the aircraft due to lift. It should be noted that:

- the correlation between the aircraft shape factor due to volume and the azimuth path angle
 is significantly affected by experimental test conditions, such as the flight path of the scaled
 model and the position of the fire trajectory with respect to the acoustic transducer;
- the correlation between the aircraft shape factor due to lift and the azimuth path angle is summarized in the lift parameter k_l ;
- the experiments are conducted at a constant Mach number. Therefore, it is necessary to estimate k_l value at the same Mach number. Considering k_l varies with Mach number introduces an approximation in the volume contribution, since the influence zone is

HYBRID SONIC BOOM SCALING CONCEPT

determined between the Mach cone, which varies with Mach number, and the aircraft. Presumably, this becomes irrelevant when investigating blunt bodies, indeed, in numerous experiments conducted, where the blunt shape forces the formation of a normal shock in front of the nose, a distribution of area normal to the free flow seems to be more appropriate [25].

Finally, if y_0 corresponds to the value of y at which the sum of the two F-functions (volume and lift) reaches its maximum value, the "global" aircraft shape factor can be calculated by Equation (16).

2.4 Sonic Boom Propagation

Whitham's modified linear theory is strictly applicable only for homogeneous media and therefore cannot account for atmospheric variations. To overcome this limitation, amplification factors can be introduced into the N-wave overpressure and duration equations presented in the previous paragraph, to allow for the propagation of the sonic boom in a standard atmosphere without winds [19]. According to Carlson, this method provides accurate results for a wide range of supersonic aircraft configurations and spacecraft operating at altitudes up to 76 km.

$$\Delta P = K_P K_R K_S \sqrt{p_v p_g} (M_{\infty}^2 - 1)^{1/8} l^{3/4} r^{-3/4}$$
(27)

$$\Delta t = K_t K_S \frac{2(\gamma + 1)}{\gamma} \frac{M_{\infty}}{a_{\nu} (M_{\infty}^2 - 1)^{1/8}} l^{3/4} r^{-1/4}$$
(28)

 K_P is the pressure amplification factor, which takes into account the influence of the standard atmosphere on a pressure disturbance. Similarly, the signature duration factor K_t consider the effect of the standard atmosphere on the N-wave duration. Finally, K_R represents the reflection factor, which generally varies from 1.8 to 2.0 [19].

3. Results and Discussion

3.1 Test Case Description

The present study focuses on a sub-scale version of the STRATOFLY MR3 configuration. The model's geometry has been modified from the original MR3 configuration [6] to make it suitable for firing range tests (Figure 5). Symmetry has been introduced to avoid asymmetric lifting effects during free-flight tests and to maintain the bottom contour. In addition, canards and fins were neglected [26].

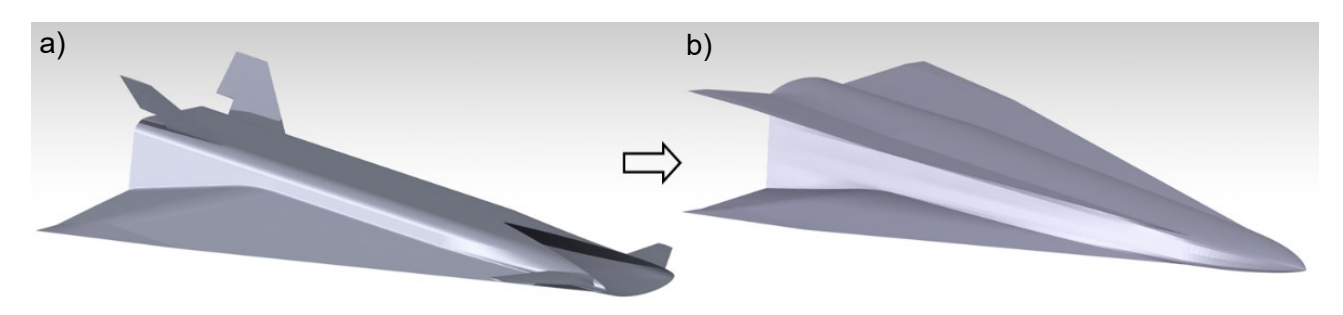


Figure 5 – STRATOFLY MR3 vehicle (a) and the free-flight model (b) [26].

The 94-meter-long waverider weighs 288 tons and reaches a nominal cruise speed of Mach 5 at approximately 30 kilometers of altitude. Instead, the scaled model used for the free-flight tests present a length of 0.2 meters and weighs only 500 grams. During the test campaign, the scaled models were launched with initial Mach numbers of about 4.7, with different initial positions and zero initial angles of attack. For more details about the experimental outdoor activity, please refer to [26]. Figure 6 shows the longitudinal area distributions of the scale model overlaid on its planform view.

Specifically, Figure 6a illustrates the volume distribution normal to the free stream, Figure 6b shows the local wingspan, and Figure 6c reports the area distribution due to lift. The lift is computed using Equation (23) and is distributed in an equal way on all 4 wings. The flow Mach number is 4.7, and the pressure at model altitude is 995 hPa.

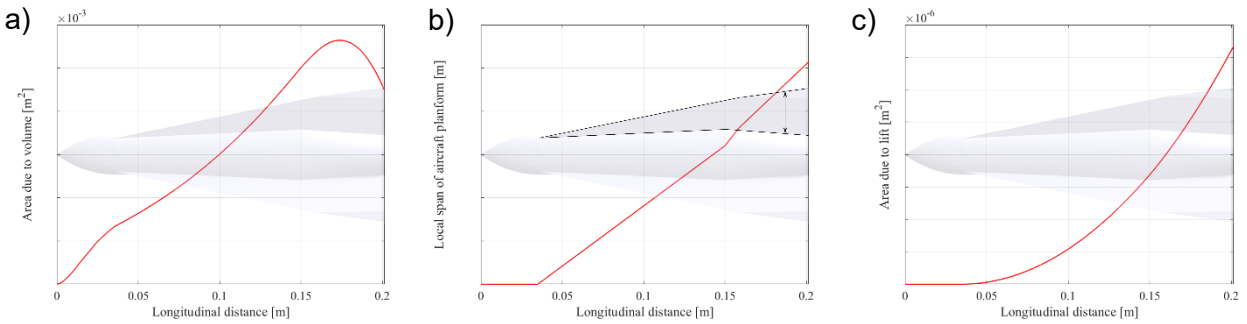


Figure 6 – Area due to volume (a), local wingspan (b) and area due to lift (c).

Although the net lift component should be zero (zero angle of attack and symmetric wings), pressure perturbation still occurs. Therefore, when quantifying the sonic boom, it is essential to consider the area distribution due to lift. However, this contribution, which is reported for demonstration purposes, has been confirmed to be negligible compared to the area distribution due to volume. The three F-functions of Figure 7, namely the Lighthill (black solid line), the Whitham (red solid line), and the Modified Lighthill (black dashed line) F-function, are calculated using the area due to volume of the scaled model (Figure 6a). The Modified Lighthill F-function, proposed by Timothy [27], introduces a correction to the weight associated with the Lighthill equation:

$$F_{L,M}(y) = \frac{1}{2\pi} \int_0^\infty \sqrt{\frac{2}{\beta R(\xi)}} h\left(\frac{y-\xi}{\beta R(\xi)} - 1\right) dA'(\xi)$$
 (29)

The interpretation of the supersonic area-rule concept at a Mach number of 4.7 presents an issue when applied to the model. The F-function (Figure 7b) assumes negative values for a significant portion of the domain, which results in the flow almost always being overexpanded, making it impossible to quantify the integral of the positive phase. However, the normal area distribution avoids such dilemma, particularly when used as input in the Lighthill F-functions. In these F-functions, in fact, the domain of influence is already controlled by the quantity $\beta R(\xi)$.

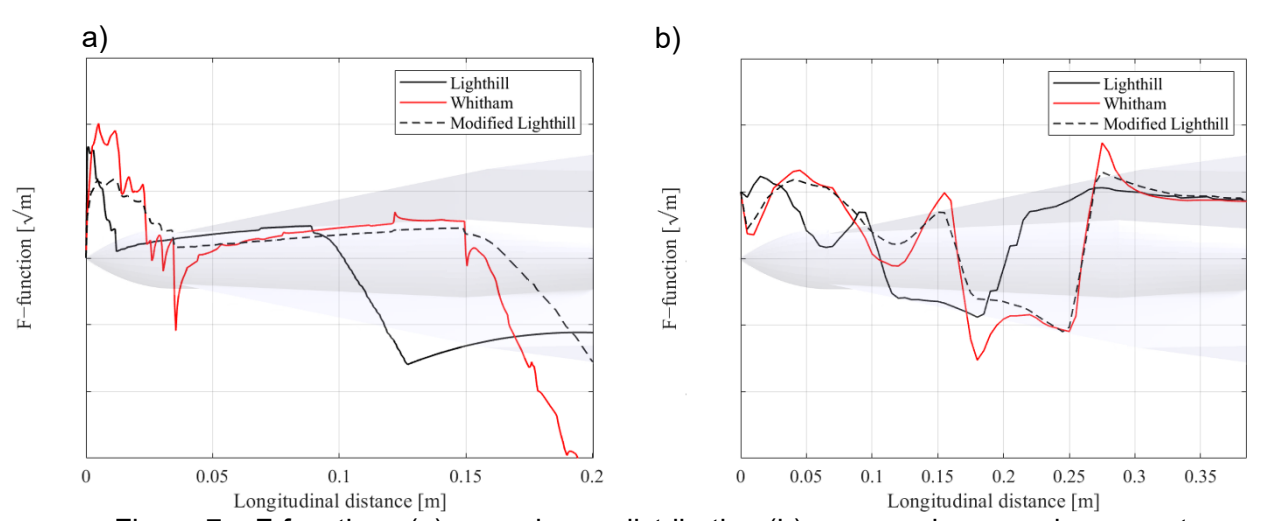


Figure 7 – F-functions (a) normal area distribution (b) supersonic area rule concept.

The analytical procedure discussed in this subsection and the results of the theoretical models are presented solely to evaluate the theoretical-experimental correlation in estimating the volume contribution to sonic boom formation. As previously explained, the impact of volume on the sonic boom of full-size aircraft will be quantified using experimental data collected during free-flight test.

3.2 Test Case Results

For each of the five free-flight tests, Figure 8 shows the pressure signatures measured with four 1/4inch pressure-field microphones at various distances from the trajectory (approximately 5 and 10 meters, enough to ensure N-wave development). The measured signatures are compared to the hybrid signatures, which are based on both theory and experiment. Specifically, they are computed using Equations (8,9), the corresponding test parameters, including Mach number, sound speed, atmospheric pressure, distance from trajectory and the hybrid F-function according to Equations (18,22). The noticeable oscillations in the measured pressure signatures are believed to be attributed to the transducer responses at high resonant frequencies, which are naturally associated with poor damping [14]. These fluctuations occur, in fact, on the leading and trailing wave of the N-signature, i.e., the part of the N-wave signal characterized by high-frequency components. Therefore, in this paper, to compensate for these limitations, the measured signatures were adjusted by introducing simple linear regressions. Specifically, only data corresponding to the linear portion of the measured N-waves were fitted. The goodness of fit (R^2) is reported in the legend of each graph. Undoubtedly, these modifications do not constitute a rigorous procedure for enhancing data quality. However, when compared to hybrid signatures, the adjusted measured signatures demonstrate a significant improvement.

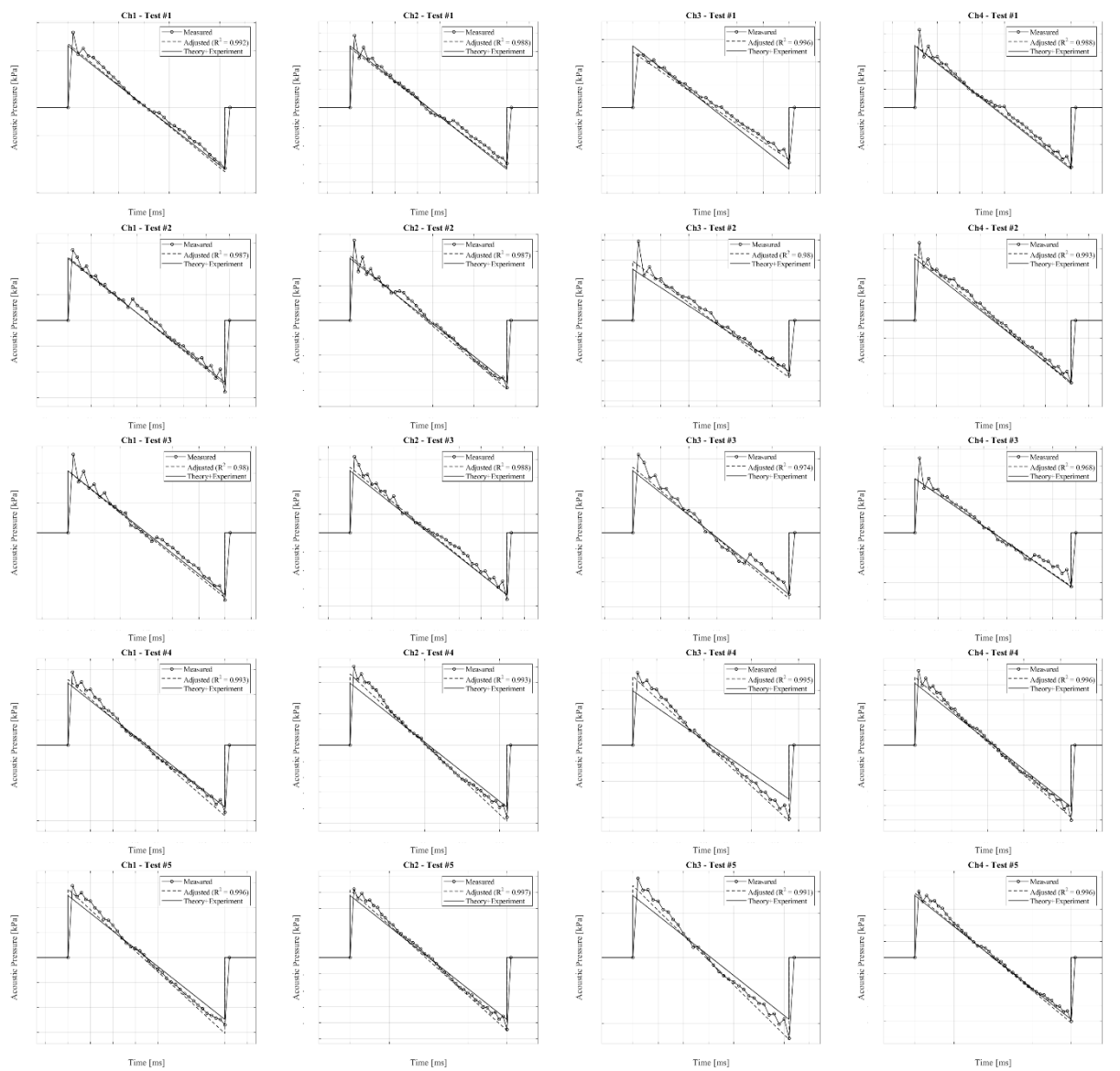


Figure 8 – Comparison of flight-test measurements and hybrid (theory+experiment) predictions of pressure signatures of the hypersonic MR3 scaled model.

The good agreement between the hybrid and adjusted signatures can be seen as evidence of the performance of the hybrid F-function approach (at least with regard to the scaled MR3).

Prior to computing the aircraft shape factors due to volume for each test and microphone it is essential to recognize that a body immersed in a real fluid flow develops a thin viscous boundary layer next to the surface, which thickens along the length of the body itself or possibly separates and encloses a flow recirculation zone, affecting the total area profile. Consequently, the hybrid F-functions calculated from experimental results will incorporate both volume and boundary layer contributions. Specifically, this is contingent on the assumption that the scaling approach considers a boundary layer thickness that scales with the same model scale. In reality, the boundary layer contribution to the total area profile becomes more significant as the scale of the model increases [28]. In any case, since the volume contribution results dominant, the aircraft shape factor derived from the experimental data would provide a reliable estimate of the sonic boom contribution due to volume for the full-size vehicle.

For each test and microphone, the aircraft shape factors due to volume can be estimated using Equations (14,18). The results are shown in the box-and-whisker plot in Figure 9.

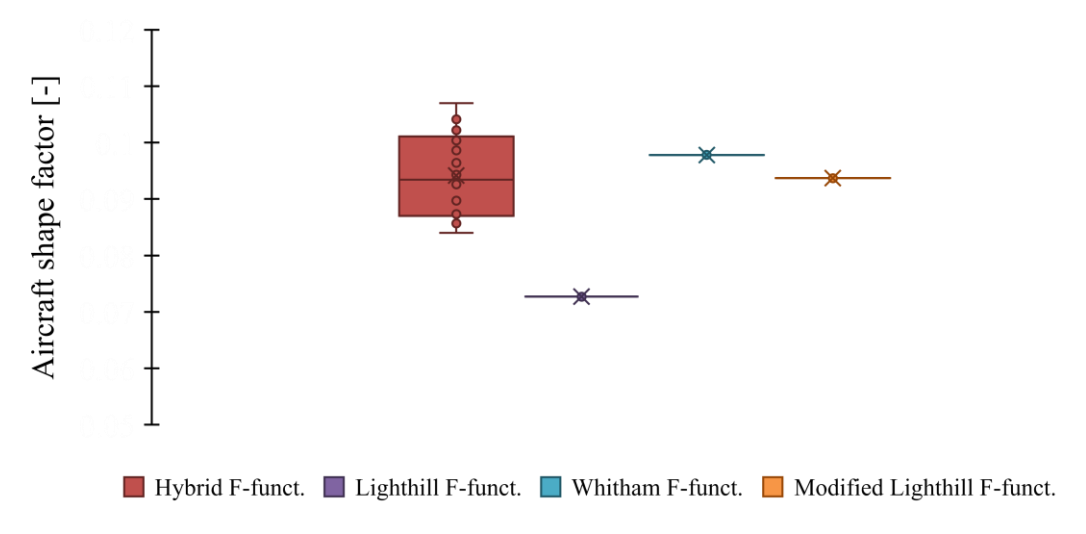


Figure 9 – Aircraft volume shape factors.

Given the various starting positions of the model and the slow rolling motion exhibited during the free-flight tests, a mean aircraft shape factor, derived from the hybrid F-functions computation, was retained the appropriate value to accurately reflect the volume contribution to sonic boom formation for the MR3 scale model. Furthermore, it is crucial to remember that if the free-flight model had been derived from a pure scaling procedure of the full-size MR3, the scaled model shape factor due to volume, as conceived, would have been identical for the full-size vehicle. However, the free-flight model was obtained by merging two scaled MR3 in a symmetrical manner. This means that the experimental responses refer to a model with twice the area distribution compared to the pure scale MR3. Therefore, to make the mean value of the aircraft shape factor due to volume meaningful, it must be divided by the square root of two.

Once the aircraft volume shape factor was obtained, the next step was to define an equivalent area due to lift, which was necessary to determine the appropriate shape factor due to lift. A detailed discussion of the theoretical methods to derive such contributions has already been presented in previous sections. The modified Lighthill F-function was selected to compute the aircraft shape factors due to lift as its demonstrated capability to predict the mean volume shape factor with considerable precision (Figure 9). Specifically, Equation (26) was employed to compute the area distribution due to lift. Equation (29) was then utilized to estimate the F-functions. Finally, Equation (15) was used to compute the aircraft shape factors due to lift as a function of the lift coefficient.

The global aircraft shape factor, obtained from the shape factors just calculated by means of Equation (16), are shown in Figure 10 (red curve) in a shape factor chart which also includes contemporary aircraft [19].

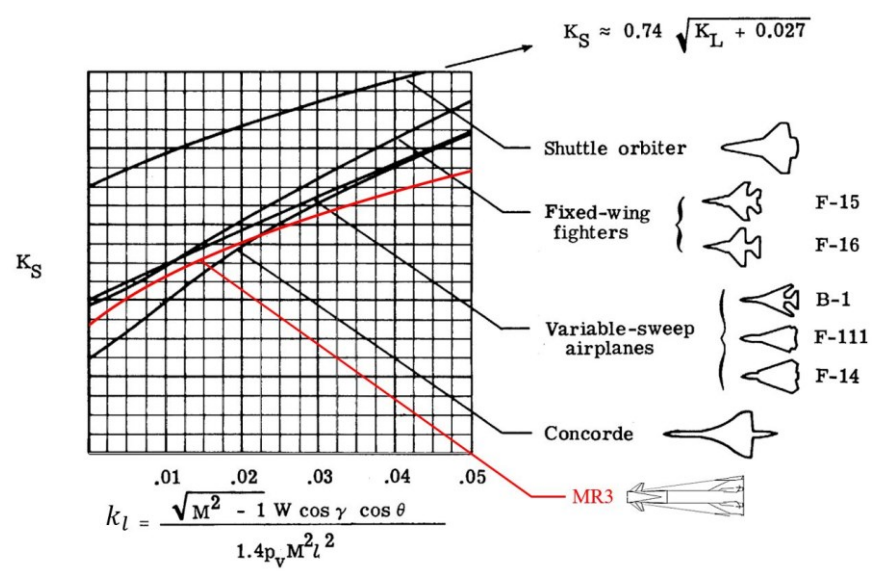


Figure 10 – Representative aircraft shape factors.

It is well-known that the application of the Whitham theory may prove inadequate at high Mach numbers due to the influence of nonlinear effects and for the simplification in considering the cross-sectional area when estimating the lift contribution. Therefore, while the presented method remains always valid for any configuration at supersonic speed, the validity of the results obtained for the hypersonic test case need to be discussed. In particular, NASA experimental studies on sonic boom phenomena [29] shown very good agreement to the flow field that should hold to within a distance of very few body lengths, for complex airplane model configuration as well as for the simple body shapes in the lower Mach number and lower lift range. Analogous consideration can be given for fairly high Mach numbers, however, considering very slender configurations (high fineness ratio). Experiments have also shown that the correlation with the linear theory improves with increasing distance (the overall pressure field disturbances become weaker and as the large distance approximations of the theory become more applicable), therefore, some improvement in correlation might be expected at large distances comparable to flight altitudes. Consequently, given that the MR3 is designed to fly at a very high altitude (30 km), has a slender geometry, and low lift coefficients (see ref. [30]), the results predicted, although the high speeds, should be quite reliable.

4. Conclusions

In this paper, a procedure was proposed to estimate the ground signature of a full-scale aircraft by combining experimental results from free-flight tests on a subscale model, theoretical estimation on the full-scale aircraft, and a simple propagation model. Assuming the most common far-field sonic boom signature, namely the N-wave, it was possible to condense the sonic boom characteristics into a single line on a parametric chart governed by the global aircraft shape factor. Typically, such a factor can be split into two contributions: one related to volume and one associated to the lift.

The experimental measurements need to be conducted in a ballistic range. The acoustic transducers should be positioned far enough from the fire line in order to fall into the far-field region and measure the N-wave signatures. Furthermore, a scaled model should be launched at a high speed. In this scenario, the area contribution due to lift can be reliably neglected, and the N-wave time duration measurements can be utilized to identify an equivalent slender right-cylinder cone of finite length that accounts for the scaled model volume contribution. Since the shape factor due to volume does not depend on the dimensions of the model, but rather on its shape, the same factor can be considered as a reliable estimate of the contribution of the full-size vehicle's volume.

With regard to the area due to lift development for the full-size aircraft, in order to evaluate the corresponding aircraft lift shape factor, a theoretical approach already available in the literature was integrated into the proposed procedure. Furthermore, in order to enhance the accuracy of the predictions, it was proposed that the area distribution resulting from lift distribution be calculated separately for each lifting surface that exhibits a comparable lift coefficient.

The data gathered during an outdoor sonic boom test campaign carried out as part of the MORE&LESS project were employed for the presented hybrid sonic boom scaling concept with the aim of obtaining a preliminary estimation of the MR3 sonic boom characteristics. The scaled model's geometry was slightly modified compared to the original MR3 configuration in order to make it suitable for firing range tests. Consequently, certain adjustments were introduced in the estimated volume aircraft shape factor.

In conclusion, the estimated MR3 global aircraft shape factors were presented in a shape factors chart which also includes contemporary aircraft.

5. Contact Author Email Address

mailto: g.fasulo@cira.it

6. Copyright Statement

The authors confirm that they, and/or their company or organization, hold copyright on all of the original material included in this paper. The authors also confirm that they have obtained permission, from the copyright holder of any third party material included in this paper, to publish it as part of their paper. The authors confirm that they give permission, or have obtained permission from the copyright holder of this paper, for the publication and distribution of this paper as part of the ICAS proceedings or as individual off-prints from the proceedings.

References

- [1] Steelant, J.: ATLLAS: Aero-thermal loaded material investigations for high-speed vehicles. In 15th AIAA International Space Planes and Hypersonic Systems and Technologies Conference, 2582 (2008).
- [2] Steelant, J., Varvill, R., Walton, C., Defoort, S., Hannemann, K., Marini, M.: Achievements obtained for sustained hypersonic flight within the LAPCAT-II project. In 20th AIAA international space planes and hypersonic systems and technologies conference, 3677 (2015).
- [3] Blanvillain, E., Gallic, G.: HIKARI: Paving the way towards high-speed air transport. In 20th AIAA International Space Planes and Hypersonic Systems and Technologies Conference 3676 (2015).
- [4] Steelant, J., Langener, T., Hannemann, K., Marini, M., Serre, L., Bouchez, M., Falempin, F.: Conceptual design of the high-speed propelled experimental flight test vehicle HEXAFLY. In 20th AIAA international space planes and hypersonic systems and technologies conference, 3539 (2015).
- [5] Steelant, J., Villace, V., Kallenbach, A., Wagner, A., Andro, J. Y., di Benedetto, S., ... & Buttsworth, D. (2018). Flight testing designs in HEXAFLY-INT for high-speed transportation. Proceedings of HiSST.
- [6] Viola, N., Fusaro, R., Saracoglu, B., Schram, C., Grewe, V., Martinez, J., ... & Fureby, C. (2021). Main challenges and goals of the H2020 STRATOFLY project. Aerotecnica Missili & Spazio, 100(2), 95-110.
- [7] Project-MORE&LESS. https://cordis.europa.eu/project/id/101006856 (2020). Accessed 1 January 2024.
- [8] Rallabhandi, S. K., Nielsen, E. J., Diskin, B.: Sonic Boom Mitigation through Aircraft Design and Adjoint Methodology, Journal of Aircraft, Vol. 51, No. 2, 2014, pp. 502-510.
- [9] Fenbert, J. W.: Conceptual Design of Low-Boom Aircraft with Flight Trim Requirement, Journal of Aircraft, Vol. 52, No. 3, 2015, pp. 932-939.
- [10]Rathsam, J., Coen, P., Loubeau, A., Ozoroski, L., & Shah, G. (2023, June). Scope and Goals of NASA's Quesst Community Test Campaign with the X-59 Aircraft. In 14th ICBEN Congress on Noise as a Public Health Problem.
- [11] Howe, D., & Henne, P. (2006). Improved sonic boom scaling algorithm. In 44th AIAA Aerospace Sciences Meeting and Exhibit (p. 27).
- [12] Maglieri, D. J., Sothcott, V. E., & Keefer Jr, T. N. (1993). Feasibility study on conducting overflight measurements of shaped sonic boom signatures using the firebee BQM-34E RPV (No. NAS 1.26: 189715)
- [13] CALLAGHAN, J. (1968). The simulation of sonic boom by ballistic models. In 3rd Aerodynamics Testing Conference (p. 383).
- [14] CALLAGHAN, J. (1966). A feasibility investigation concerning the simulation of sonic boom by ballistic models (Test program to determine feasibility of laboratory simulation of sonic boom by ballistic models). 1966. 97 P.
- [15] Whitham, G. B. (1952). The flow pattern of a supersonic projectile. Communications on pure and applied mathematics, 5(3), 301-348.
- [16] Hayes, W. D. (1947). Linearized supersonic flow (Doctoral dissertation, California Institute of Technology).

HYBRID SONIC BOOM SCALING CONCEPT

- [17] Walkden, F. (1958). The shock pattern of a wing-body combination, far from the flight path. Aeronautical quarterly, 9(2), 164-194.
- [18] Ritzel, D. V., & Gottlieb, J. J. (1987). The overpressure signature from a supersonic projectile. UTIAS Report, No. 279.
- [19] Carlson, H. W. (1978). Simplified sonic-boom prediction (No. NASA-TP-1122).
- [20] Jung, T. P., Starkey, R. P., & Argrow, B. (2012). Methodology for Conducting Scaled Sonic-Boom Flight Tests Using Unmanned Aircraft Systems. Journal of aircraft, 49(5), 1234-1244.
- [21] D. J. Maglieri, Sonic Boom: Six Decades of Research, Langley Research Center, 2014.
- [22] Carlson, H. W., Mack, R. J., & Morris, O. A. (1966). Sonic-boom pressure-field estimation techniques. The Journal of the Acoustical Society of America, 39(5B), S10-S18.
- [23] Carlson, H. W., & Maglieri, D. J. (1972). Review of sonic-boom generation theory and prediction methods. The Journal of the Acoustical Society of America, 51(2C), 675-685.
- [24] De Luca, D. (2020). Sub-Transonic and Supersonic STRATOFLY MR3 Aerodatabase development by means of CFD Simulations (Doctoral dissertation, Politecnico di Torino).
- [25] Carlson, H. W., & Mack, R. J. (1978). A wind-tunnel study of the applicability of far-field sonic-boom theory to the space shuttle orbiter (No. NASA-TP-1186).
- [26] Fasulo, G., Hengy, S., Martinez, B., Federico, L., De Vivo, L., Albisser, M., Zeiner, A. Experimental Outdoor Activity on Sonic Boom Assessment of the STRATOFLY MR3 Scale Model (2024). Proceedings of HiSST.
- [27] Jung, T. P. (2012). Modified Linear Theory Aircraft Design Tools and Sonic Boom Minimization Strategy Applied to Signature Freezing via F-function Lobe Balancing (Doctoral dissertation, University of Colorado at Boulder).
- [28] Krasnov, N. F., & Morris, D. N. (1970). Aerodynamics of bodies of revolution (pp. 239-263). American Elsevier Publishing Company.
- [29] Schwartz, I. R. (Ed.). (1971). Third conference on sonic boom research (Vol. 255). Scientific and Technical Information Office, National Aeronautics and Space Administration.
- [30] Viola, N., Roncioni, P., Gori, O., & Fusaro, R. (2021). Aerodynamic characterization of hypersonic transportation systems and its impact on mission analysis. Energies, 14(12), 3580.